https://doi.org/10.1016/j.compstruct.2019.111846

Finite element modeling of 3D spacer fabric: effect of the geometric variation and amount of spacer yarns

Yuan Zhang[1], Hong Hu[2], Yordan Kyosev[3], Yanping Liu[1*]

[1]Engineering Research Center of Technical Textile of Ministry of Education, College of Textiles, Donghua University, Shanghai, China

[2]Institute of Textiles and Clothing, The Hong Kong Polytechnic University, Hong Kong, China

[3]Institute of Textile Machinery and High Performance Material Technology (ITM), Technische Universität Dresden, Dresden, Germany

*Corresponding Author

Email: liuyp@dhu.edu.cn

Abstract:

3D spacer fabrics are a type of sandwich structure consisting of two separate multifilament fabric outer layers linked together with a layer of spacer monofilaments. They have been widely used as energy absorbing materials and composite reinforcement. The microstructure features and compression behavior of a typical spacer fabric were investigated experimentally and numerically in this study. Eight unit cells with 64 spacer monofilaments were reconstructed from scanning of the fabric via Micro X-ray computed tomography (μCT). The geometric variations of the reconstructed spacer monofilaments were analyzed quantitatively. It was found that spacer monofilaments in different unit cells are different in length, curvature and torsion. A series of FE models based on different numbers and combinations of the identified unit cells were created. The FE simulation results showed that the geometric variations of spacer monofilaments have strong influence on the compression behavior, and the model with shorter length, lower curvature and torsion of spacer monofilaments has higher compression resistance. The compression resistance in the densification stage of the fabric increases with increasing the number of spacer monofilaments adopted due to more evident interactions among spacer yarns. This study provides an in-depth understanding into the compression behavior of spacer fabric.

Keywords: spacer fabric; compression behavior; finite element analysis; monofilament

1. Introduction

3D spacer fabrics are a type of sandwich structure consisting of two separate outer layers which are connected by one layer of spacer yarns, as shown in Fig. 1(a) [1]. They are produced with double-needle bar Raschel warp knitting machines of low cost, high productivity and large structural variety. As illustrated in Fig.1(c) and (d), the two outer layers are normally knitted with pliant polyester multifilaments to have a flexible structure, while the spacer layer is knitted with relatively coarse polyester monofilaments which are anchored into the out layers to link them together and serve as the main load carrier under compression, as shown in Fig.1 (b). The spacer monofilaments can be either vertical or inclined to form I, X or IXI configurations, among which IXI is the most used one due to its good stability as illustrated in Fig. 1 (b). Since the monofilament loops are stuck between the overlap and underlap of the outer layers, highly complicated binding and boundary conditions are created for the spacer yarns orienting in the thickness direction. Besides, neighboring monofilament loops in the wale direction are also intermeshed, providing further fixation for the spacer yarns. Hence, 3D spacer fabrics composed of both soft and rigid components are an integrated composite structure with complex internal constraints, giving rise to a highly anisotropic and nonlinear mechanical behavior. The in-plane mechanical behavior of spacer fabrics is flexible, but the through-the-thickness compression resistance can be tailored by either manipulating spacer monofilament architecture and materials or changing outer layer knitted structures to modify the binding conditions. While the space between the two outer layers can be varied from 1 mm to 65 mm, the loop density of the outer layers on the machine can be adjusted from 6 to 24 loops/inch. These special structural features give spacer fabrics the possibility to have a wide range of structural variations and physical and mechanical properties. For instance, the

use of spacer monofilaments with different diameters or stiffness can bring the spacer fabrics with different compression resistance, and the creation of open-hole structures on each outer layer can achieve high air circulation for comfort purpose.

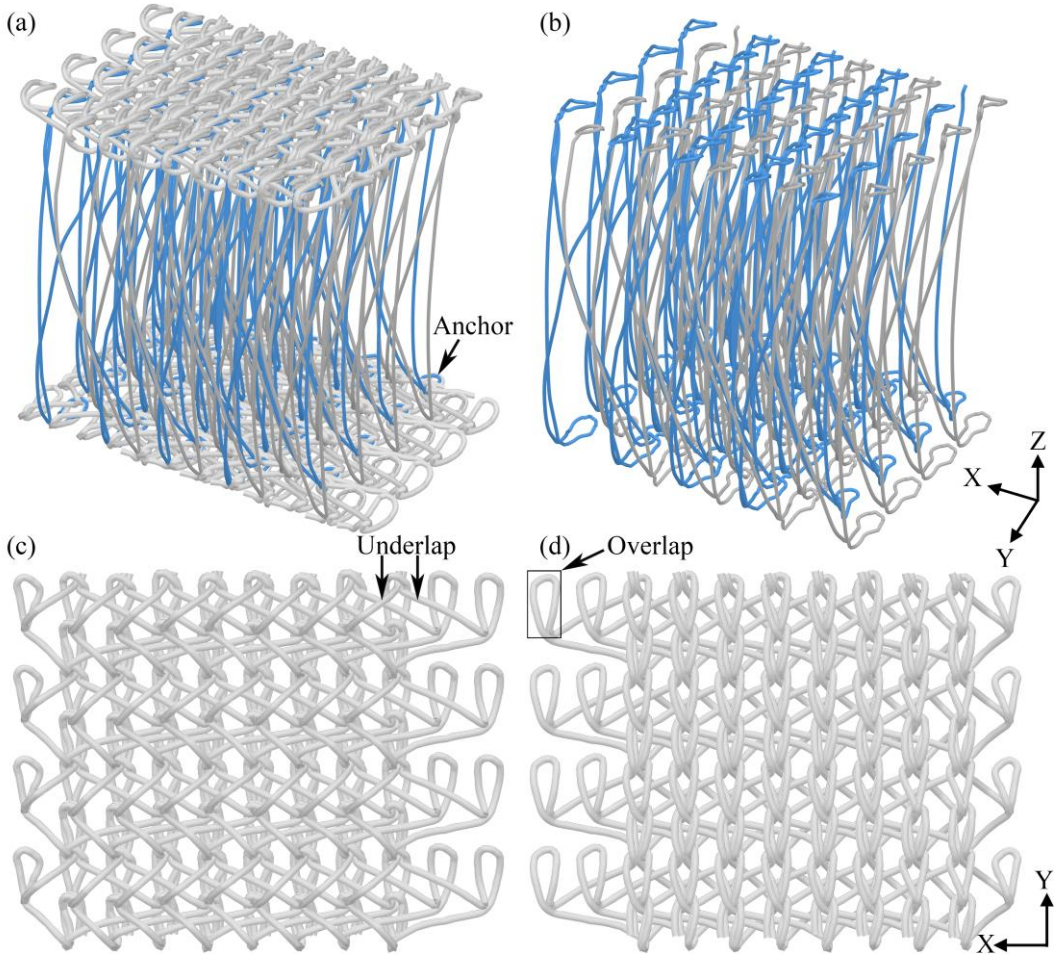

Fig. 1. The micro-structure of a 3D spacer fabric: (a) complete structure; (b) spacer layer; (c) internal side of outer layer; (d) external side of outer layer.

By selecting appropriate multifilament and monofilament materials, yarn architectures, and structural parameters, spacer fabrics can be engineered to have a wide range of energy-absorbing properties to meet the requirements of different applications. In fact, spacer fabrics have already been used as cushioning materials for replacing polymeric foams in the development of automotive interior, cushion pads, mattresses, and impact

protectors, etc. The demand of high quality spacer fabrics is increasing dramatically in recent years, especially in automotive industry.

Extensive experimental studies have been conducted to investigate the compression behavior of spacer fabrics produced with different structures and yarn materials as cushioning materials for various applications such as car seats [2], insoles [3], bra cup [4], impact protectors [5-7], vibration isolators [8], or as reinforcement for composite materials such as textile reinforced concrete [9,10], polyurethane foam [11], and shear thickening fluid [12]. It has been found that 3D spacer fabrics can be developed to have the key features of a cushioning material like polymeric foam having three distinct stages under compression, which are characterized by linear elasticity, plateau and densification. Post-buckling, torsion, shear, rotation and contacts of the spacer monofilaments as well as the contacts between the spacer monofilaments and outer layers were observed in the experiments [5]. These multiple and complex deformation modes come from the fabric's complex and discontinuous structure which demonstrates highly nonlinear compression behavior. Liu et al. found that a thinner spacer fabric knitted with coarser spacer monofilaments more oriented to the thickness direction and bound by tight outer layer structures has higher compression resistance [5, 6].

The prototyping process of spacer fabrics with the required mechanical properties is time-consuming and high cost due to the complex manufacturing processes and multiple structural variables. A thorough understanding of the compression behavior and structure–property relationships of spacer fabrics is vital for rationally selecting structural parameters and yarn materials for a specific application. Theoretical studies

can provide an efficient way to analytically or numerically predict the compression behavior of spacer fabrics so as to reduce cost and carry out exact design to meet specific requirements. Pervious analytical studies for spacer fabrics had developed models based on the Euler-Bernoulli beam theory to predict the post-buckling behavior of a single spacer monofilament by neglecting its interaction with other spacer monofilaments [13–17]. Finite element (FE) method is a practical and effective way to simulate the compression of spacer fabrics by taking internal contacts into consideration. Vassiliadis et al. created a FE model to simulate the post-buckling deformation of spacer monofilaments without considering the interaction among fabric components [18]. Brisa et al. reported a FE model for a single vertical spacer monofilament of a thick spacer fabric under compression by taking the contacts between the spacer monofilaments and the outer layers into account [19]. Hou et al. also conducted a FE study on a spacer fabric by considering the contacts between the spacer monofilaments and outer layers, in which the initial geometric shapes of the spacer monofilaments of a unit cell were calculated by a nonlinear buckling analysis from the manufacturing parameters, and the outer layers were treated as two isotropic planes [20,21]. Sun et al. presented a parametric FE study on a spacer fabric by simplifying the spacer yarns as identical, vertical and linearly elastic rods and adjusting the structural parameters to investigate the structure-property relationship [22]. Orlik et al. developed a homogenization and dimension reduction technique to predict the effective elastic properties of spacer fabrics [23]. Liu et al. reported a FE study on the compression behavior of a typical spacer fabric structure based on the precise geometry of a unit cell reconstructed from μCT scanning by fully considering the yarn interactions among all the fabric components and material's nonlinearity, and a satisfactory prediction of the compression load–displacement relationship of the fabric

was achieved [24]. However, only one unit cell with a limited number of spacer monofilaments was included in their model. Besides, the geometric variation of spacer yarns and the constraints exerted by surrounding unit cells were not studied. These simplifications made the model unable to provide a complete compression mechanism of the spacer fabric.

This work presents a further FE study aiming at providing a deeper insight into the compression behavior of spacer fabrics by including the geometric variations of spacer monofilaments and varying the number of unit cells. At the same time, the yarn interactions and nonlinear material properties were fully taken into consideration in the FE simulations. It is expected that the finding obtained in this study could give a comprehensive understanding on the compression mechanism of spacer fabrics.

2. Geometric analysis of the spacer fabric

A typical 3D spacer fabric with spacer yarn configuration "IXI" which was knitted on a GE296 double-needle bar Raschel machine with six yarn guide bars was used for this study [25]. The fabric thickness is 7.52 mm and its density is 134.08 kg/m^3. The two outer layers of the fabrics were separately knitted with four sets of 300D/96F polyester multifilaments, while the other two sets of polyester monofilaments with 0.2 mm diameter were used to join the two outer layers together in a single knitting process. A 3D geometry of this fabric was created by using the software EAT ProCad Warpknit as illustrated in Fig. 1.

The structural features of the fabric were examined by using a microscope (HITACHI TM3000) and a μCT system (Scanco/VivaCT 40, SCANCO Medical AG, Switzerland).

Fig. 2 shows the side view from walewise and the internal structures. The two separate outer layers are linked together with the spacer monofilaments in both vertical and inclined forms (Fig. 2 (a) and (b)), and the monofilament overlaps are covered and wrapped by the fluffy multifilament overlaps and underlaps (Fig.2 (c) and (d)). The monofilament overlaps are almost concealed by the multifilament loops from both external and internal sides, providing a stable constraint for the spacer monofilaments. However, some heterogeneity in binding conditions exists. As can be seen from Fig. 2(c) and (d), some of the monofilament loops are visible. This definitely affects the initial geometric shapes of the spacer yarns although the fabric has a periodic structure. It is necessary to note that both the vertical and inclined spacer yarns are different from one to another. Different initial spacer yarn shapes and different binding conditions exerted on them concurrently affect the fabric mechanical properties. The binding conditions can be changed by deformation of spacer yarns and vice versa, so that the coupling effect between the binding conditions and spacer yarn deformation is extremely complex. In this regard, unlike conventional sandwich structures and materials, the spacer fabric structure is highly heterogeneous and discontinuous.

The heterogeneous nature of the fabric might result from uneven yarn mechanical properties, inconsistent yarn tensions during knitting, and different degrees of wearing on the needles. Since these factors cannot be eliminated, geometric variations of spacer monofilaments are inevitable. It is of great importance to know the degree of geometric variation among spacer monofilaments and how those variations would affect the fabric compression behavior.

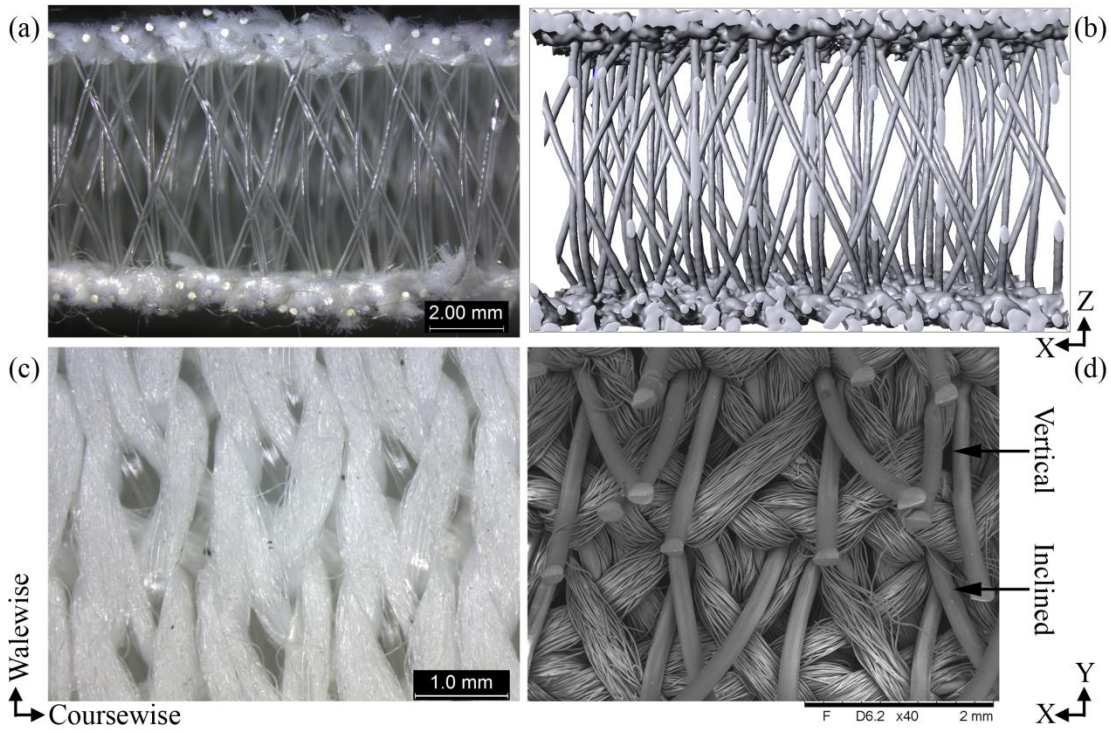

Fig. 2. Photographs of the spacer fabric: (a) microscopic side view; (b) μCT reconstruction side view; (c) external side of outer layer; (d) internal side of outer layer.

In order to get precise geometry of the spacer fabric, scanning through its thickness direction was carried out by using a μCT system. The slice thickness and pixel size were 0.021mm. One of the slices obtained from the scanning is shown in Fig. 3, where the white dots represent the cross-sections of spacer monofilaments. A binarization processing was applied to obtain a better visualization which demonstrates a periodic pattern. It is easy to identify the unit cells each of which includes 8 spacer monofilaments, despite some variations among the unit cells [24]. One of the unit cells (U2) was selected to visualize a 3D unit cell spacer layer as shown in Fig. 4. Each unit cell consists of two pairs of vertical (v1, v2 and v5, v6) and two pairs of inclined (i3, i4 and i7, i8) spacer monofilaments as annotated in Fig. 4. Each pair of the spacer monofilaments is located in the same course. While the vertical spacer monofilaments

are roughly parallel, the inclined ones are crossed each other, forming a relatively stable structure. Fig. 4(c) clearly reveals that both the vertical and inclined spacer yarns in the same unit cell have different initial shapes. The vertical spacer yarns v5 and v6 are more torsional than v1 and v2, which means that the later pair of yarns are more vertical as shown in Fig. 4(a). The inclined spacer yarns of the same pair have different curvatures and are not fully symmetrical. These features could partly impair the stability of the whole fabric structure.

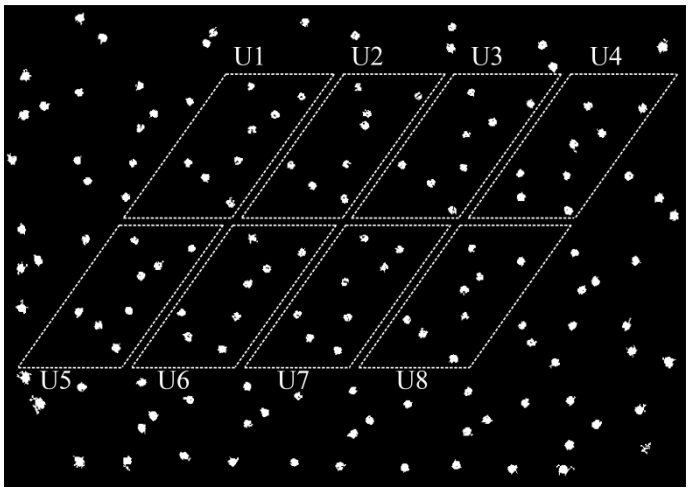

Fig. 3. A binarized slice from μCT scanning with 8 identified unit cells.

Fig. 5 presents the projections of each of 8 monofilaments in the X-Y plane in the identified 8 unit cells. Intuitively, spacer monofilaments in different unit cells differ considerably from one to another. The shapes of spacer monofilaments at the same locations in different unit cells are basically similar. For instance, all the spacer monofilaments v5 and v6 of the 8 unit cells projected in Fig. 5(e) and (f) are self-intersecting curves with different enclosed areas. The geometric variations of the spacer monofilaments are quantitatively assessed in terms of length, curvature and torsion, as well as similarity.

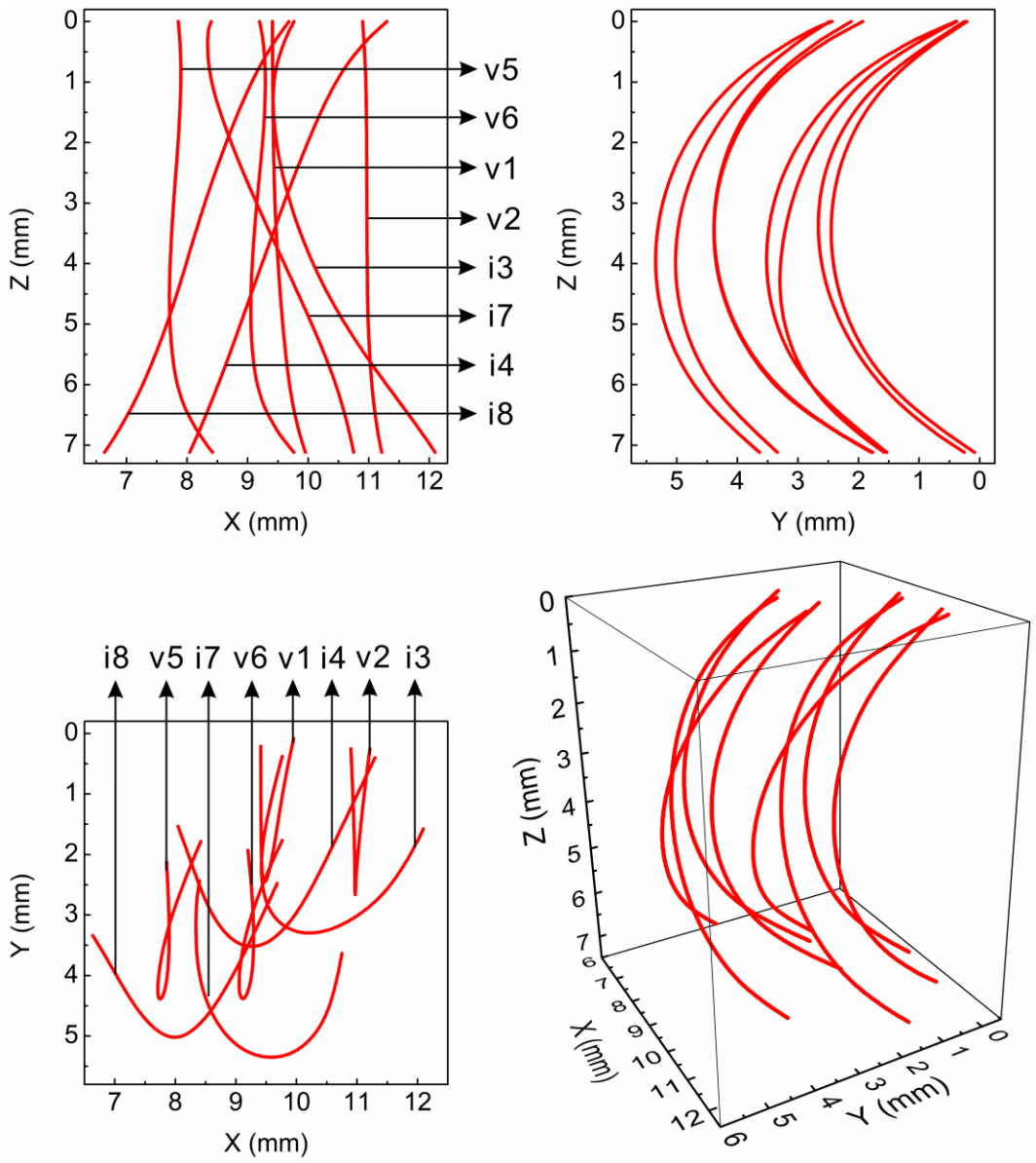

Fig. 4. 3D Plots of eight spacer monofilaments in the unit cell U2.

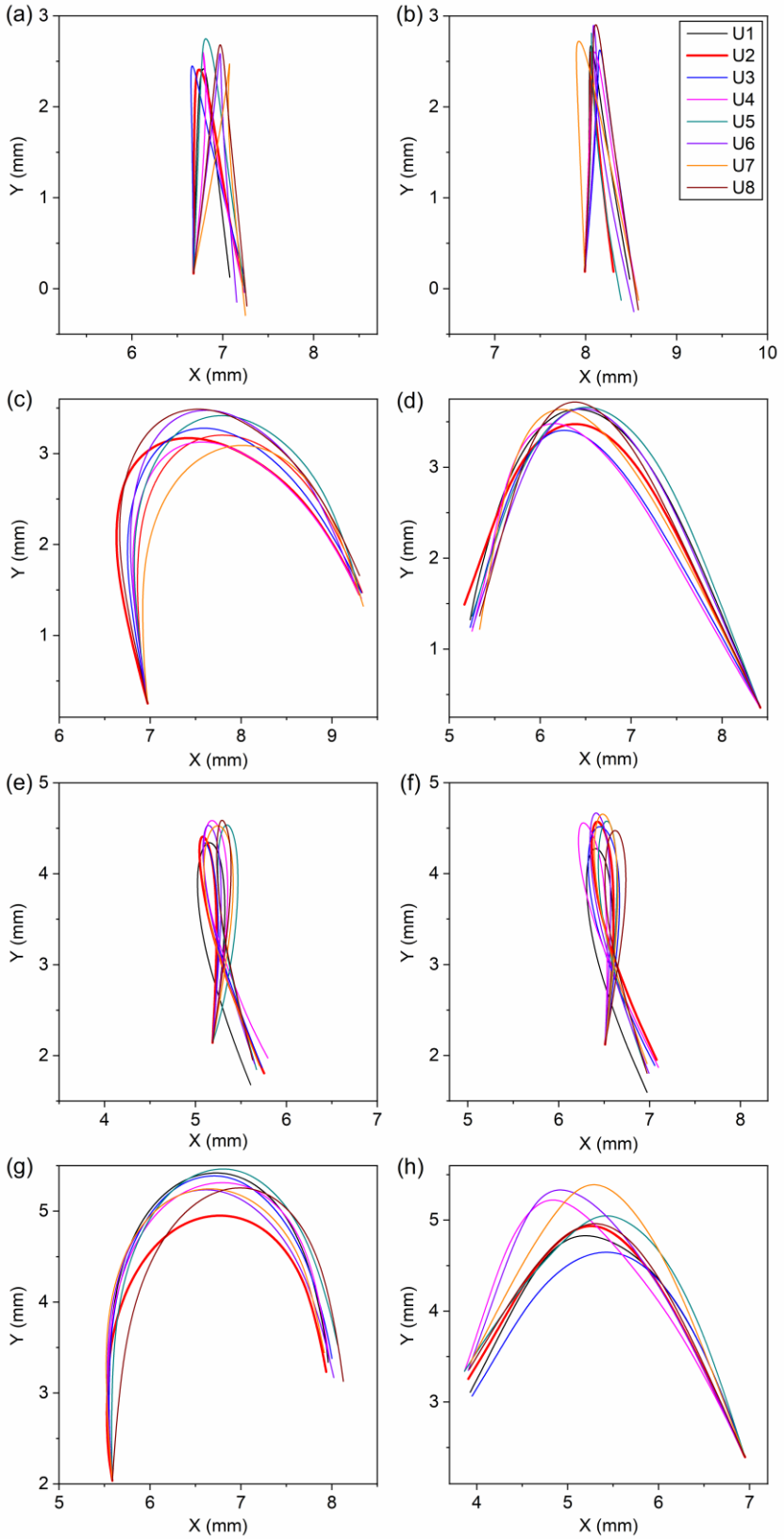

Fig. 5. Projections of eight spacer monofilaments in the eight unit cells in the X-Y plane: (a)v1; (b)v2; (c)i3; (d)i4; (e)v5; (f)v6; (g)i7; (h)i8.

2.1 Length of spacer monofilaments

The spacer yarn length mainly depends on the distance of two needle beds, knitting sequence, spacer yarn arrangement, yarn mechanical property and individual yarn tension. Table 1 lists the respective length of the spacer yarns in the 8 unit cells. The lengths of those spacer yarns in different unit cells are not identical. The reasons for this phenomenon are complicated. This might be due to the fact that the mechanical property of spacer monofilament is not perfectly identical throughout the length. Inconsistent yarn tensions during warping and knitting, different needle positions and different degrees of wearing on the needles are also possible reasons for the discrepancies among spacer yarns.

It is also found Table 1 that the inclined yarns are normally longer than the vertical yarns. This is because the inclined spacer yarns crossing three needles consume more yarns than the vertical spacer yarns which are only fed between two opposite needles. Since the monofilaments are running at a constant speed during the knitting process, the inclined spacer yarns with higher yarn consumption will have higher yarn tension than the vertical spacer yarns with lower yarn consumption. Yarn tension regulators installed on the machine ensure a smooth tension transition from knitting of the vertical spacer yarns to the inclined ones. It should be noted that this tension discrepancy also affects the shape and length of monofilament overlaps anchored into the outer layers.

Table 1. Lengths of spacer yarns in the eight unit cells

Unit cell	Length of spacer yarn (mm)								
	v1	v2	i3	i4	v5	v6	i7	i8	Sum
U1	8.88	9.17	9.49	10.18	9.25	9.23	9.93	9.20	75.33
U2	8.94	9.04	9.61	9.84	9.23	9.37	9.38	9.16	74.57
U3	8.90	9.20	9.66	9.91	9.08	9.37	9.90	8.94	74.96
U4	9.29	9.29	9.41	10.03	9.41	9.45	9.86	9.53	76.27
U5	9.52	9.58	9.84	10.15	9.33	9.39	9.82	9.31	76.94
U6	9.35	9.84	9.79	10.18	9.31	9.56	9.81	9.67	77.51
U7	9.34	9.50	9.37	10.27	9.36	9.46	9.64	9.68	76.62
U8	9.49	9.81	9.82	10.17	9.34	9.30	9.82	9.15	76.9
Average	9.21	9.43	9.62	10.09	9.29	9.39	9.77	9.33	-
SD	0.27	0.30	0.19	0.15	0.10	0.10	0.18	0.27	-

2.2 Curvature and torsion of spacer monofilaments

The differences in yarn consumptions and tensions in knitting the vertical and inclined spacer yarns resulted in different curvatures and torsions. Spacer yarns deforming from straight lines to nonlinear and nonplanar space curves experienced two tension changing steps; one is on the machine and the other is off the machine. Initially, tensional vertical spacer yarns were straight without any curvature and torsion on the machine. Once the lapping motion for knitting the vertical yarns was completed, the tension was released and swiftly altered for knitting the succeeding inclined yarns. In this transition, deviation from straight line and planarity was formed on the vertical spacer yarns. In the same way, curved and torsional inclined spacer yarns were also

formed subsequently. After the fabric was removed from the machine for further processing, external tension exerted on the fabric was eliminated. The fabric shrunk in width, length and thickness at the same time which further enlarged the curvature and torsion of spacer monofilaments. After that, the fabric was subject to heat setting under tension. The fabric was extended in the horizontal direction to a required width, run into a stenter for heat treatment and then cooled down in order to fix the geometry. Spacer monofilaments underwent further shrinkage in this process which could impart additional deviations of curvature and torsions to spacer monofilaments. Hence, the formation of spacer fabrics was a highly uncertain post-buckling process which could be affected by uneven yarn material properties and asymmetrical internal forces, leading to considerable geometric variations of spacer monofilaments.

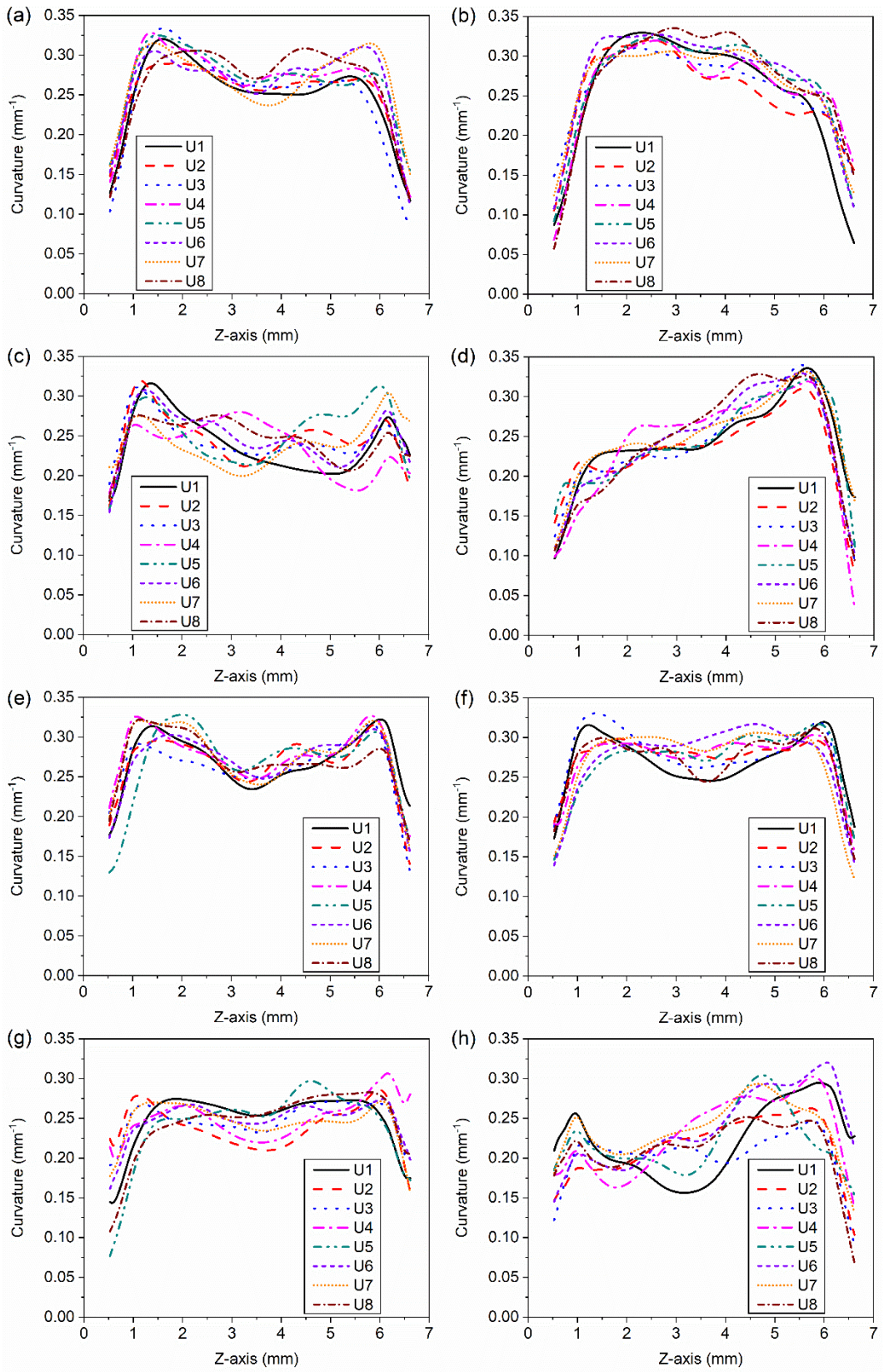

Fig. 6. The curvatures of eight monofilaments in eight unit cells: (a)v1; (b)v2; (c)i3; (d)i4; (e)v5; (f)v6; (g)i7; (h)i8

The curvatures and torsions of the spacer monofilaments in the 8 unit cells were calculated. Fig. 6 shows that curvatures of the spacer yarns vary nonlinearly through the thickness from 0.034 to 0.362 mm^{-1}. The vertical spacer yarns are comparatively symmetrical, and their curvatures increase from the two endpoints to the middle sections. In the middle sections, the curvatures fluctuate between 0.25 and 0.35 mm^{-1}. The curvatures of the inclined spacer yarns vary through the thickness in a similar way, but not as symmetrical as the vertical spacer yarns. It also appears that the curvatures of spacer yarns in different unit cells are varied. Fig. 7 shows torsions of the spacer yarns through the thickness. The variations in torsion are more complicated than those in curvature. The torsion curves differ markedly with a low degree of regularity. It can be either positive or negative, indicating different directions of twisting. Since the curvature and torsion are changed through the thickness and they jointly determine a space curve, it is hard to directly relate them to fabric compression resistance. For this reason, the statistic results of curvature and torsion are evaluated and listed in Table 2 and Table 3, respectively. The mean value of curvature can be considered as a direct measure to compare different spacer monofilaments. It is interesting to note that the sum of the curvature mean of eight spacer yarns has the same order as that of spacer yarn length listed in Table 1. This implies that a unit cell with lower total spacer yarn length has lower mean curvature. By contrast, the torsion statistics have no clear order as the curvature data.

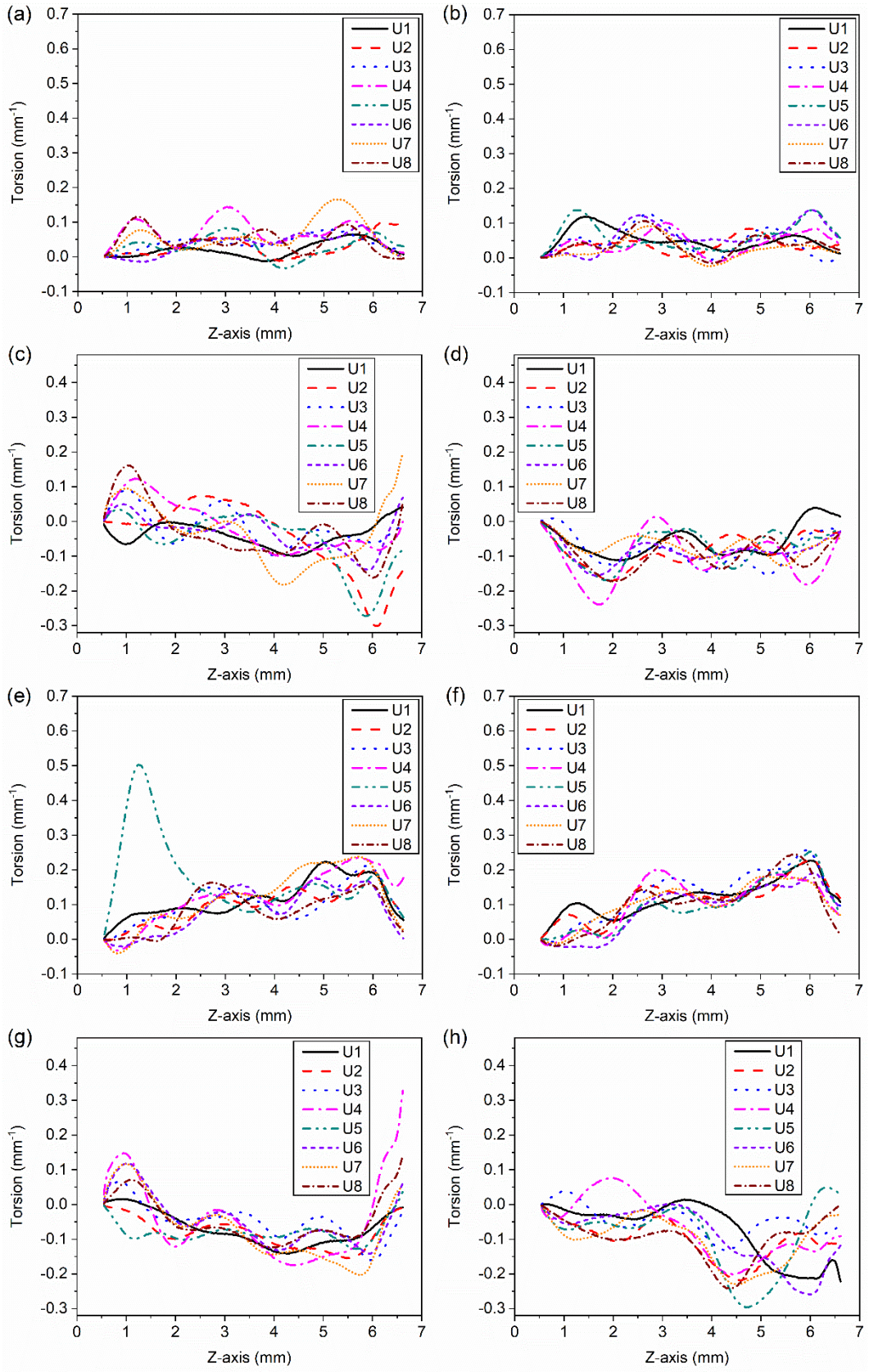

Fig. 7. The torsion of eight monofilaments in eight unit cells: (a)v1; (b)v2; (c)i3; (d)i4; (e)v5; (f)v6; (g)i7; (h)i8

Table 2. Curvature statistics of the spacer yarns in the eight unit cells

Unit cell	Spacer yarn	Curvature (mm^{-1})			Unit cell	Spacer yarn	Curvature (mm^{-1})		
		min	mean	max			min	mean	max
U1	v1	0.117	0.254	0.320	U5	v1	0.154	0.272	0.325
	v2	0.064	0.260	0.329		v2	0.092	0.274	0.323
	i3	0.168	0.241	0.316		i3	0.157	0.255	0.313
	i4	0.097	0.246	0.336		i4	0.110	0.247	0.324
	v5	0.177	0.272	0.322		v5	0.130	0.273	0.328
	v6	0.173	0.273	0.320		v6	0.146	0.274	0.317
	i7	0.144	0.251	0.275		i7	0.077	0.245	0.297
	i8	0.156	0.222	0.295		i8	0.153	0.222	0.304
	sum	1.096	2.019	2.513		sum	1.019	2.062	2.531
U2	v1	0.121	0.256	0.290	U6	v1	0.109	0.270	0.310
	v2	0.105	0.259	0.321		v2	0.108	0.280	0.327
	i3	0.161	0.248	0.319		i3	0.154	0.250	0.308
	i4	0.076	0.235	0.310		i4	0.101	0.248	0.330
	v5	0.141	0.271	0.316		v5	0.157	0.273	0.310
	v6	0.164	0.276	0.298		v6	0.139	0.278	0.317
	i7	0.158	0.240	0.286		i7	0.161	0.250	0.275
	i8	0.103	0.217	0.263		i8	0.145	0.240	0.320
	sum	1.029	2.002	2.403		sum	1.074	2.089	2.497
U3	v1	0.082	0.254	0.334	U7	v1	0.150	0.270	0.315
	v2	0.148	0.264	0.310		v2	0.125	0.270	0.308
	i3	0.189	0.245	0.311		i3	0.200	0.240	0.304
	i4	0.093	0.242	0.340		i4	0.110	0.254	0.332
	v5	0.132	0.266	0.317		v5	0.161	0.279	0.321
	v6	0.144	0.280	0.331		v6	0.122	0.277	0.306
	i7	0.191	0.249	0.271		i7	0.157	0.247	0.272
	i8	0.090	0.206	0.247		i8	0.131	0.238	0.294
	sum	1.069	2.006	2.461		sum	1.156	2.075	2.452
U4	v1	0.122	0.269	0.328	U8	v1	0.116	0.271	0.309
	v2	0.069	0.265	0.320		v2	0.058	0.276	0.335
	i3	0.178	0.237	0.280		i3	0.172	0.247	0.276
	i4	0.033	0.245	0.319		i4	0.093	0.249	0.329
	v5	0.175	0.279	0.327		v5	0.167	0.274	0.322
	v6	0.156	0.277	0.304		v6	0.147	0.274	0.312
	i7	0.199	0.250	0.307		i7	0.108	0.248	0.283
	i8	0.138	0.232	0.303		i8	0.068	0.215	0.252
	sum	1.07	2.054	2.488		sum	0.929	2.054	2.418

Table 3. Torsion statistics of the spacer yarns in the eight unit cells

Unit cell	Spacer yarn	Torsion (mm^{-1})			Unit cell	Spacer yarn	Torsion (mm^{-1})		
		min	mean	max			min	mean	max
U1	v1	-0.013	0.023	0.065	U5	v1	-0.033	0.037	0.084
	v2	0.003	0.052	0.119		v2	0.001	0.062	0.139
	i3	-0.100	0.044	0.041		i3	-0.273	0.065	0.034
	i4	-0.112	0.065	0.040		i4	-0.170	0.074	-0.002
	v5	0.003	0.117	0.224		v5	0.014	0.177	0.503
	v6	0.004	0.121	0.227		v6	-0.001	0.099	0.253
	i7	-0.142	0.073	0.016		i7	-0.128	0.082	0.037
	i8	-0.222	0.075	0.014		i8	-0.297	0.100	0.048
	sum	-0.579	0.57	0.746		sum	-0.887	0.696	1.096
U2	v1	-0.012	0.031	0.101	U6	v1	-0.015	0.040	0.090
	v2	0.001	0.035	0.085		v2	-0.006	0.062	0.138
	i3	-0.302	0.080	0.075		i3	-0.141	0.045	0.068
	i4	-0.171	0.085	-0.003		i4	-0.157	0.086	0.000
	v5	-0.002	0.098	0.205		v5	-0.021	0.090	0.175
	v6	0.002	0.118	0.228		v6	-0.025	0.098	0.190
	i7	-0.155	0.084	-0.002		i7	-0.142	0.076	0.119
	i8	-0.219	0.104	-0.002		i8	-0.259	0.090	0.001
	sum	-0.858	0.635	0.687		sum	-0.766	0.587	0.781
U3	v1	0.000	0.042	0.079	U7	v1	0.000	0.062	0.167
	v2	-0.010	0.049	0.126		v2	-0.025	0.029	0.093
	i3	-0.100	0.048	0.090		i3	-0.183	0.075	0.194
	i4	-0.152	0.086	0.010		i4	-0.127	0.071	-0.001
	v5	0.000	0.103	0.211		v5	-0.041	0.126	0.238
	v6	-0.009	0.133	0.256		v6	-0.012	0.109	0.182
	i7	-0.161	0.060	0.066		i7	-0.204	0.098	0.118
	i8	-0.132	0.055	0.039		i8	-0.025	0.102	-0.004
	sum	-0.564	0.576	0.877		sum	-0.617	0.672	0.987
U4	v1	0.004	0.071	0.144	U8	v1	-0.006	0.049	0.115
	v2	-0.012	0.044	0.101		v2	-0.016	0.040	0.107
	i3	-0.101	0.065	0.124		i3	-0.162	0.073	0.161
	i4	-0.239	0.107	0.013		i4	-0.173	0.093	-0.001
	v5	-0.033	0.126	0.236		v5	-0.005	0.085	0.164
	v6	-0.017	0.111	0.201		v6	-0.020	0.108	0.245
	i7	-0.176	0.107	0.327		i7	-0.124	0.073	0.143
	i8	-0.202	0.092	0.077		i8	-0.242	0.100	-0.003
	sum	-0.776	0.723	1.223		sum	-0.748	0.621	0.931

By connecting the two endpoints of each spacer monofilament projected in the X-Y plane, the enclosed areas are calculated and listed in Table 4. The area is an indirect but intuitive measure for the torsion level of vertical spacer yarns and curvature level of inclined spacer yarns. It is found that U2 has the smallest enclosed area among the 8 unit cells. In this connection, U2 is chosen as the standard sample for assessing the similarity among different unit cells.

Table 4. Enclosed area of spacer monofilaments' projective curves in the X-Y plane

Unit cell	Enclosed area (mm^2)								
	v1	v2	i3	i4	v5	v6	i7	i8	Sum
U1	0.52	0.61	4.72	5.69	0.46	0.43	5.49	4.09	21.99
U2	0.70	0.32	4.99	5.05	0.40	0.48	4.61	3.90	20.44
U3	0.63	0.66	4.95	4.91	0.37	0.58	5.36	3.79	21.26
U4	0.52	0.76	4.58	4.99	0.54	0.50	5.35	4.28	21.53
U5	0.85	0.36	5.30	5.64	0.45	0.42	5.39	4.29	22.71
U6	0.58	0.49	5.08	5.52	0.41	0.45	5.36	4.47	22.35
U7	0.62	0.87	4.54	5.31	0.56	0.48	5.05	4.54	21.97
U8	0.82	0.85	5.41	5.21	0.39	0.45	5.29	3.88	22.29
SD	0.13	0.21	0.32	0.30	0.07	0.05	0.28	0.28	-

2.3 Similarity of spacer monofilaments

The Fréchet distance is a measure of similarity between two curves *p* and *q*, which is defined as the minimum cord-length sufficient to join a point traveling forward along *p* and one traveling forward along *q*, although the rate of travel for either point may not

necessarily be uniform. A parameterized curve in $\mathbb{R}^d$ can be described as a function p: [0, 1]$\rightarrow \mathbb{R}^d$. A monotone reparametrization α is a continuous non-decreasing function α: [0,1] $\rightarrow$[0,1] with $\alpha(0)=0$ and $\alpha(1)=1$. For the two curves p, q: [0, 1] $\rightarrow \mathbb{R}^d$, the Fréchet distance between them is expressed as:

$$\delta_F(p,q) := \inf_{\alpha,\beta} \max_{t\epsilon[0,1]} d\left(p(\alpha(t)), q(\beta(t))\right) \quad (1)$$

where d(p, q) denotes the Edulidean distance between points traveling p and q; α and β range over all monotone reparametrizations[26]. The Fréchet distances between each of the 3D space curves reconstructed from the 8 spacer monofilaments in U2 and the relevant one in the other 7 unit cells are listed in Table 5. The data show that U1 and U3 are more similar to U2. Particularly, vertical spacer yarns v1, v2, v5 and v6 of U2 and U3 are very similar with relatively low Fréchet distances.

Table 5. The similarity of 3D space curves of spacer monofilaments

Unit cell	3D Fréchet distance (mm)								
	v1	v2	i3	i4	v5	v6	i7	i8	Sum
f12	0.17	0.20	0.52	0.18	0.20	0.38	0.47	0.16	2.28
f23	0.13	0.28	0.28	0.26	0.08	0.09	0.45	0.32	1.89
f24	0.22	0.41	0.30	0.31	0.21	0.16	0.37	0.49	2.46
f25	0.36	0.33	0.46	0.25	0.30	0.16	0.52	0.23	2.61
f26	0.30	0.50	0.47	0.27	0.15	0.17	0.33	0.51	2.70
f27	0.36	0.42	0.61	0.32	0.24	0.11	0.32	0.46	2.86
f28	0.36	0.51	0.39	0.25	0.28	0.22	0.37	0.11	2.49
SD	0.10	0.11	0.12	0.05	0.08	0.10	0.08	0.16	-

3. FE Analysis

The uneven discontinuous outer layers impose complex restraints on the spacer monofilaments, and those spacer monofilaments also have substantial geometric variations, jointly creating a highly nonlinear compression behavior. Since it is difficult to observe the intricate interactions among the two outer layers and a large number of spacer monofilaments through experimental approach, identifying the complex compression mechanism of spacer fabrics is challenging. The restraints applied onto the spacer monofilaments by outer layers were numerically studied in the previous work [24]. This study, by contrast, focused on revealing how geometric variations of spacer monofilaments and the number of unit cells in the FE simulation could affect the fabric compression behavior.

3.1 FE models

The discontinuous outer layers were simplified as two isotropic plates capable of interacting with the spacer monofilaments. The 8 unit cells were used to establish FE models with different combinations of unit cells as illustrated in Fig. 8. Eighteen FE models containing different number of unit cells were created using the commercial finite element code ANSYS 14.5 and their definitions are given in Table 6. Fig. 9 presents one of the FE models M64 created with 8 unit cells and 64 spacer yarns as an example to describe the details. Two square plates were meshed with the shell element SHELL181 for the two outer layers. Square meshes of side length 0.2 mm were used for all the shell elements. The 64 reconstructed spacer monofilaments of the 8 unit cells were meshed by using the beam element BEAM188 with a circular section of 0.1 mm in radius. For meshing the beam elements, the circular section was divided into 20 sectors and each sector was further divided into 2 elements. Forty elements in total were used for one cross section and each beam element has a thickness of 0.021

mm.

Multipoint constraint (MPC) approach was used to connect the beams to the two shells by generating internally coupling equations. The endpoints of each beam were set as pilot nodes (TARGE170), while shell nodes within the areas occupied by the respective monofilament overlaps of the two outer layers were selected and set as contact nodes (CONTA175). Each pilot node was connected to the corresponding contact nodes to form a force-distributed constraint MPC contact pair. Force or displacement was transmitted between each pilot node and the contact nodes in an average sense, while the translational and rotational degree of freedoms (DOFs) at the beam endpoints could be constrained. As the fabric was compressed along the Z-axis (UZ), there are no translational DOFs along the X- and Y-axes (UX and UY) at the beam endpoints. The rotational DOF about the X-axis (ROTX) of spacer yarns exists because their endpoints are located at the voids formed by overlaps in the outer layers as demonstrated in Fig. 2(d). In the previous work [24], the validated FE model constrained the rotational DOFs about the Y- and Z-axes (ROTY and ROTZ) for vertical spacer yarns, but ROTY and ROTZ for inclined spacer yarns were free.

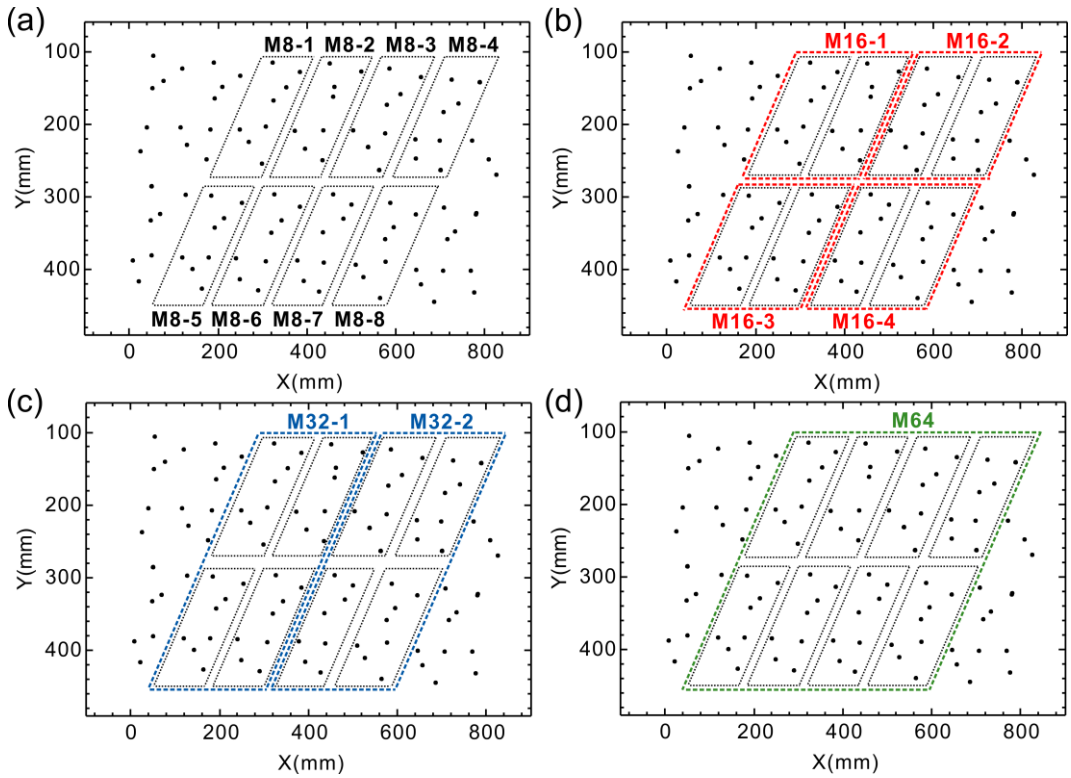

Fig. 8. Different combinations of unit cells for FE models: (a) models formed with one unit cell; (b) models formed with two unit cells; (c) models with four unit cells; (d) model with eight unit cells

Table 6. Definitions for FE models with different combination of unit cells

FE model	Unit cells	No. Unit cell	No. Spacer yarns	Outer layer sizes (mm)		
				X	Y	Z
M8-1	U1	1	8	11	11	0.2
M8-2	U2	1	8	11	11	0.2
M8-3	U3	1	8	11	11	0.2
M8-4	U4	1	8	11	11	0.2
M8-5	U5	1	8	11	11	0.2
M8-6	U6	1	8	11	11	0.2
M8-7	U7	1	8	11	11	0.2
M8-8	U8	1	8	11	11	0.2
M16-1	U1,U2	2	16	14	11	0.2
M16-2	U3,U4	2	16	14	11	0.2
M16-3	U5,U6	2	16	14	11	0.2

M16-4	U7,U8	2	16	14	11	0.2
M16*	U2,U2	2	16	14	11	0.2
M32-1	U1,U2,U3,U4	4	32	15	14	0.2
M32-2	U5,U6,U7,U8	4	32	15	14	0.2
M32*	U2×4	4	32	15	14	0.2
M64	U1,…,U8	8	64	21	14	0.2
M64*	U2×8	8	64	21	14	0.2

Note: * denotes that the model is built by repeating U2

3.2 Contact pairs

The contacts between the spacer monofilaments and outer layers as well as those among the spacer monofilaments were taken into account by creating three different contact pairs.

The interactions between the beams and shells are detected by two flexible-to-flexible line-to-surface standard contact pairs. Two contact layers (TARGE170) were placed on the two shell internal surfaces and contact elements (CONTA177) were placed on the 64 beams (Fig. 9). The shell thickness and beam radius were taken into account and the friction coefficient used was μ=0.28. The interactions among spacer monofilaments are simulated by a flexible-to-flexible line-to-line standard contact pair with μ=0.28. To form this self-contact pair, both contact elements (CONTA176) and target elements (TARGE170) were placed onto the beams. The contact between two compression platens (TARGE170) and two fabric surfaces (CONTA174) are simulated by using two rigid-to-flexible surface-to-surface bonded contact pairs without relative motion. The two compression platens are non-deformable rigid bodies, but the two fabric outer layers are deformable. A pilot node was defined on each rigid compression platen to apply the boundary conditions. A displacement of 5.6 mm in the Z direction is applied to the top platen to simulate the static compression

test, and the bottom platen is fixed by constraining all the DOFs.

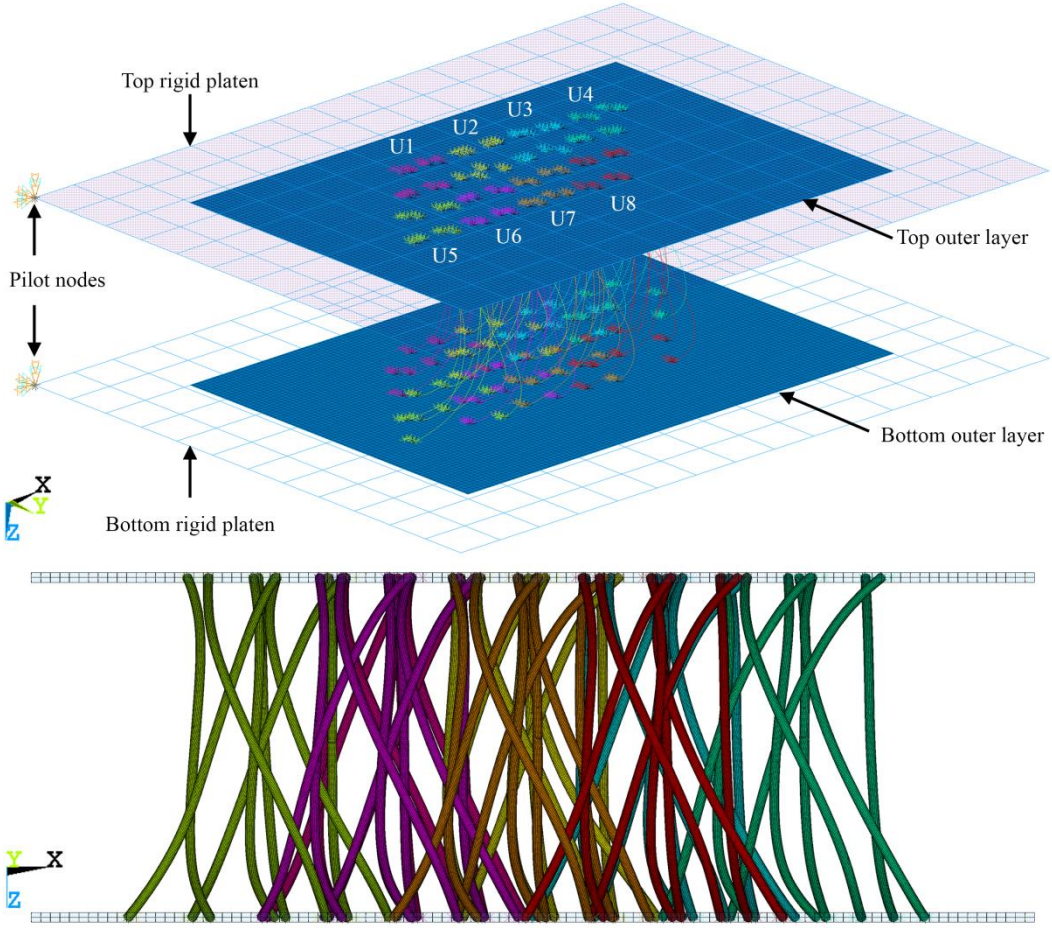

Fig. 9. FE model set-up for the spacer fabric under compression.

3.3 Material models

The tensile stress–strain curves of the polyester monofilament are shown in Fig. 10 with a Young's modulus of 12833 MPa. The nonlinear multilinear kinematic hardening model was used for the beam elements with a Poisson's ratio of 0.3 [27, 28]. A linear elastic model, i.e., a Young's modulus of 12833 MPa and a Poisson's ratio of 0.3, was defined for the shell elements because the outer layers have small deformations. The friction coefficient of the polyester monofilament (μ) was 0.28[24].

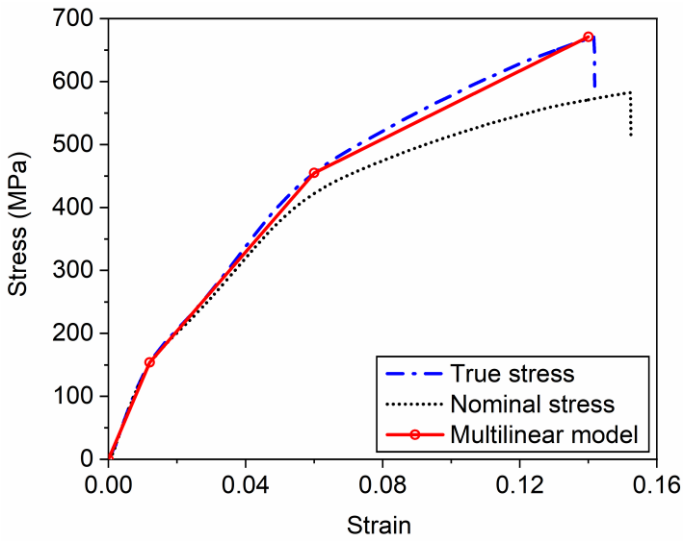

Fig. 10. Tensile stress–strain curves and multilinear kinematic hardening model of polyester monofilament.

4. Results and discussions

4.1 Effects of geometric variations of spacer monofilaments

Fig. 11 presents the compression load–displacement curves calculated by the FE models constructed from different unit cells and their combinations as defined in Fig. 8 and Table 6. The loads were multiplied to match the number of spacer monofilaments in a square spacer fabric of size 10 cm x 10 cm. An experimental curve is also included for comparison.

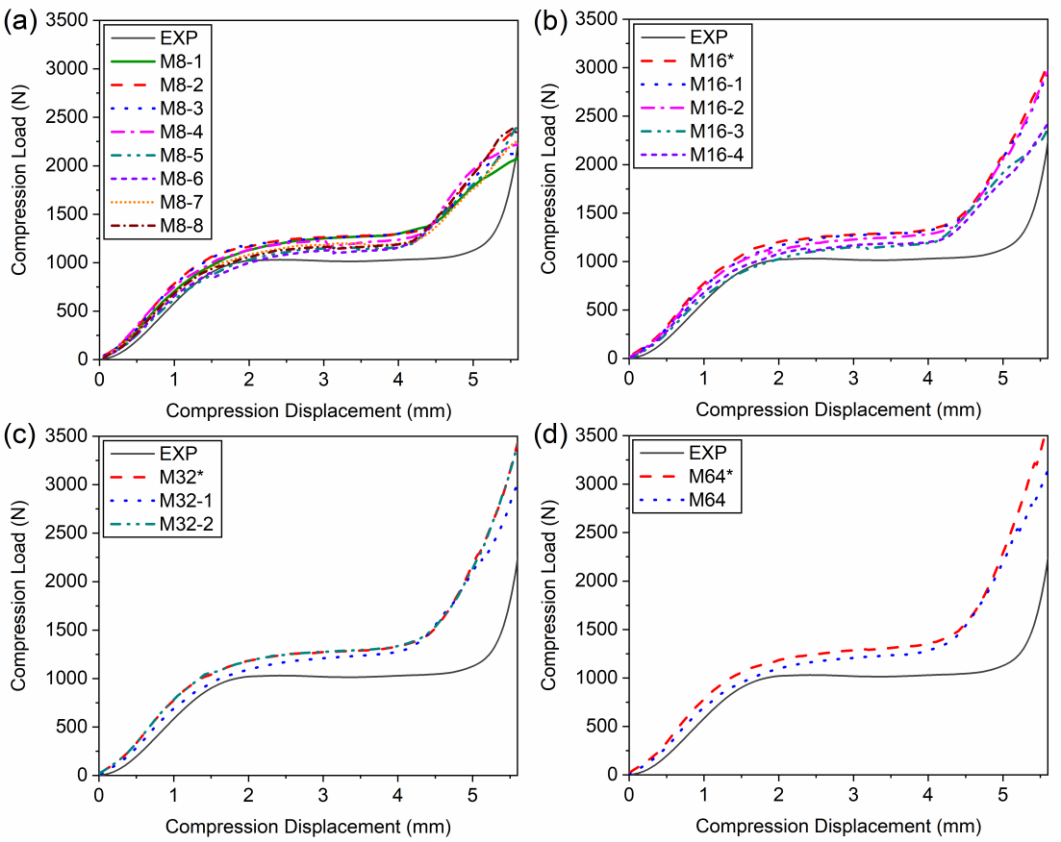

Fig. 11. Compression load–displacement curves of FE models with different unit cell combinations: (a) models formed with one unit cell; (b) models formed with two unit cells; (c) models with four unit cells; (d) model with eight unit cells.

All the eight curves in Fig. 11(a) for the FE models built with different single unit cells have similar shapes with three distinct stages: linear elasticity, plateau and densification, which are close to the experimental curve. In addition, the loads of the eight curves vary in all the three stages due to the geometric variations. This indicates that each unit cell possesses the cushioning feature independently and geometric variations of spacer monofilaments have significant effects on the compression resistance. Specifically, M8-2 has the highest compression resistance among the eight FE models built with single unit cell. This is because a shorter elastic rod with lower curvature and torsion has lower post-buckling force [6]. By referring to Table 1 and

Table 4, the unit cell U2 for M8-2 has the shortest total length and smallest enclosed area of the eight spacer monofilaments. Their curvatures and torsions are also relatively low as confirmed in Table 2 and Table 3. The similarity results in Table 5 indicate that U1 and U3 are similar to U2. They have similar spacer yarn lengths, curvatures and torsions. This explains why the compression resistance of M8-1 and M8-3 is analogous to that of M8-2. Especially, the curves of M8-2 and M8-3 are almost identical. It is found that the compression resistance increases as the total length and enclosed area decrease.

The results for the FE models built with two and four unit cells shown in Fig. 11(b) and Fig. 11(c), respectively, are also inconsistent with the rule. M16-1 and M16-2 of lower spacer yarn length and enclosed area have higher compression resistance than M16-3 and M16-4. M16* with two U2 has the greatest compression resistance among all the models built with two unit cells. For the FE models with 4 unit cells, the compression resistance of M32-1 built with U1, U2, U5 and U6 is lower than that of M32-2 built with U3, U4, U5 and U6 as shown in Fig. 11(c). This is because U5 and U6 have longer spacer yarns and higher enclosed area than the others. The compression resistance of M32* with four U2 is very close to that of M32-2. There is no doubt that M64* built with eight U2 possesses higher compression resistance than M64 constructed with real geometries (Fig. 11(d)).

In summary, all the FE models have similar compression load–displacement curves with three distinct stages, regardless of geometric variations of spacer yarns among unit cells and different combinations of unit cells. However, the geometric variations bring about different compression load levels in the three stages. Compression load is

directly related to the total length and enclosed area of spacer yarns. Low curvature and torsion of spacer yarns result in a higher compression load.

4.2 Effects of number of unit cells

Two groups of FE models with different number of unit cells were chosen to investigate how the number of spacer monofilaments in a fabric can affect the compression behavior. Fig. 12(a) shows that the compression loads in linear elasticity and plateau stages decrease as the number of spacer monofilaments increases, but those in densification stage are just the opposite. It is also found that increasing the number of spacer yarns can decrease the differences in simulated load–displacement curves.

To eliminate the effect of geometric variations, U2 was used to construct four FE models with 8, 16, 32, and 64 spacer monofilaments and the results are shown in Fig. 12(b). It can be seen that the four FE models have almost the same compression load–displacement curves in the linear elasticity and plateau stages, followed by different slopes in the densification stages. The two groups of simulation curves reveal that geometric variations of spacer yarns mainly influence the elasticity and plateau stages, and the number of spacer monofilaments has prominent effect on the densification stage. In other words, an increase in the number of spacer yarns is not likely to intensify the linear elasticity and plateau stages, but certainly enhance the compression resistance in the densification stage. This is because the interactions among spacer yarns in the first two stages are not evident, but contacts among spacer yarns in the final stage play an important role in affecting the compression behavior.

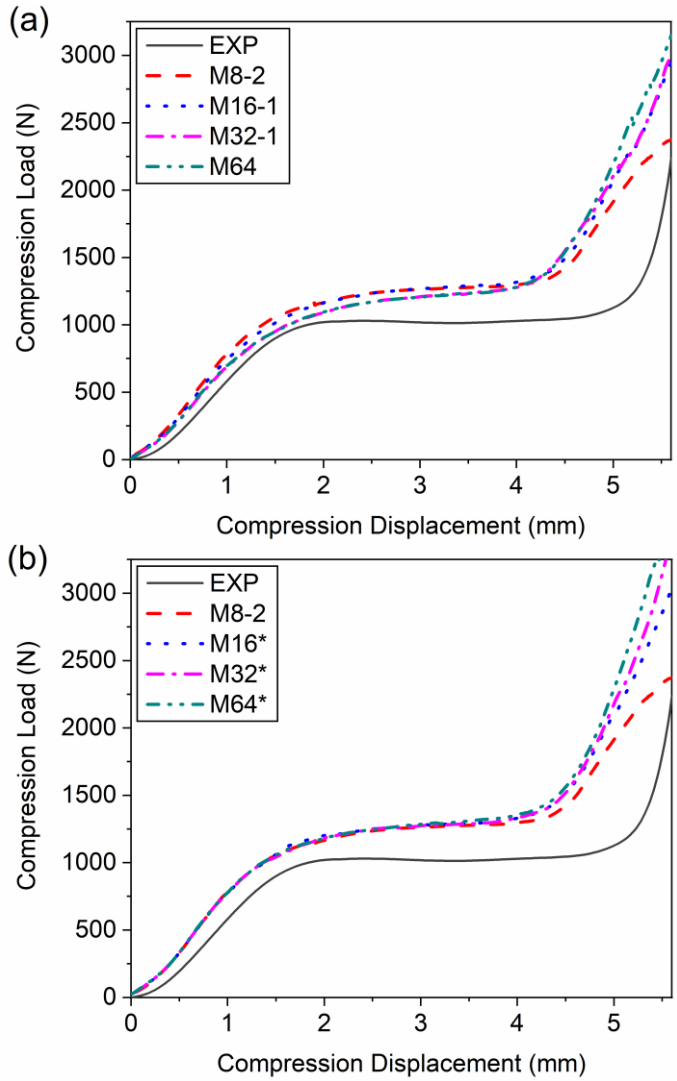

Fig. 12. Compression load–displacement curves of FE models with different numbers of unit cells: (a) real geometry; (b) repeating U2.

This phenomenon can be confirmed by visualizing the simulated interactions among spacer yarns. The FE models M8-2, M16-1, M32-1 and M64 all include the unit cell U2. Fig. 13 and Fig. 14 present the Von Mises stress (VMS) plots of U2 in the four FE models at displacements of 2.5 mm and 5 mm, respectively. It can be seen from Fig. 13 that the eight spacer monofilaments in the four models deformed similarly at the displacement of 2.5 mm which is located at the plateau stage. Adding more spacer monofilaments into models has little change on the deformation modes in the linear

elasticity and plateau stages. On the contrary, Fig. 14 shows distinct differences in deformation of spacer monofilaments at the displacement of 5 mm, belonging to the densification stage. The spacer yarn v1 in M8-2 is inclined to the left, while v1 in the other models are nearly vertical. The inclination of v6 decreases as the number of unit cell increases. Thus, the model built with more unit cells has greater compression resistance in the densification stage. It is necessary to note that the maximum Von Mises stresses of the vertical spacer yarns are all located at the middle sections with high curvatures.

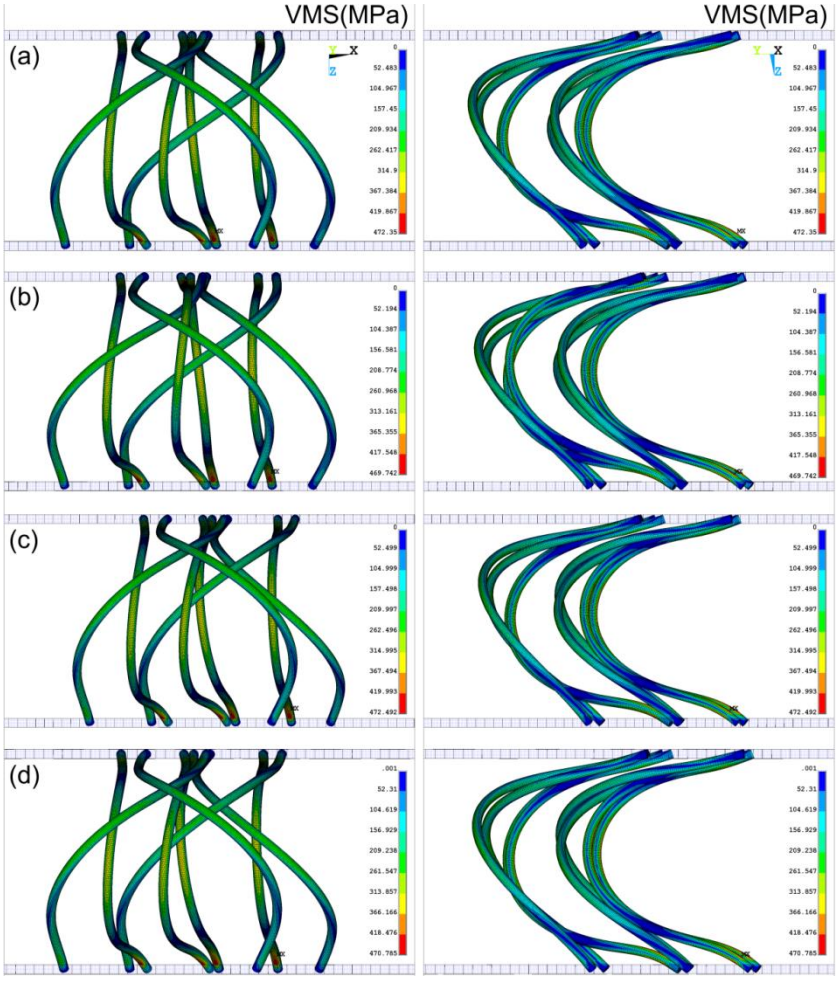

Fig. 13. Von Mises stress plots of U2 for FE models with different number of unit cells at displacement of 2.5 mm: (a) M8-2; (b) M16-1; (c) M32-1; (d) M64.

In order to have an intuitive view, the projections of deformed spacer monofilaments of U2 in the X-Y plane are shown in Fig. 15 and Fig. 16. The undeformed spacer monofilaments are also included for comparison. Differences in deformation of spacer monofilaments in the four models are quite clear. It is confirmed that the variations in deformed geometries at 5 mm are more significant than those at 2.5 mm.

The main deformation mode of spacer yarns at the displacement of 2.5 mm in the plateau stage is rotation which only has slight effect on the compression resistance. For instance, the projections of v1 for the four models in Fig. 15(a) are similar, but their rotation degrees are different. The projections of v2, v5 and v6 in different FE models nearly coincide. There are also some discrepancies in projections of inclined spacer yarns. Their deformed shapes are similar with different rotations.

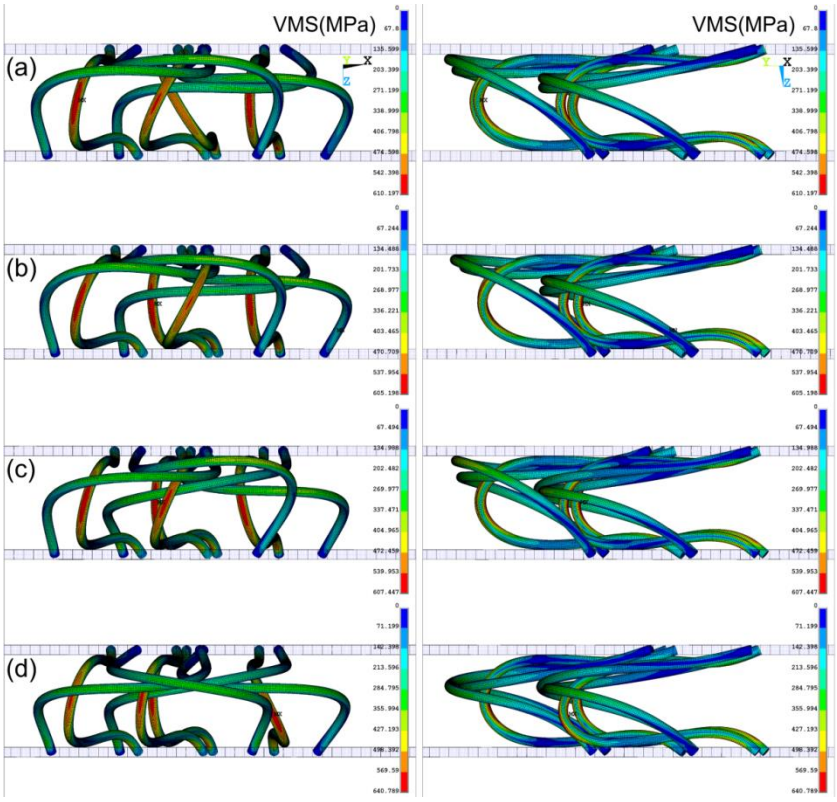

Fig. 14. Von Mises stress plots of the same unit cell (U2) in different FE models when compressed to 5mm: (a) M8-2; (b) M16-1; (c) M32-1; (d) M64.

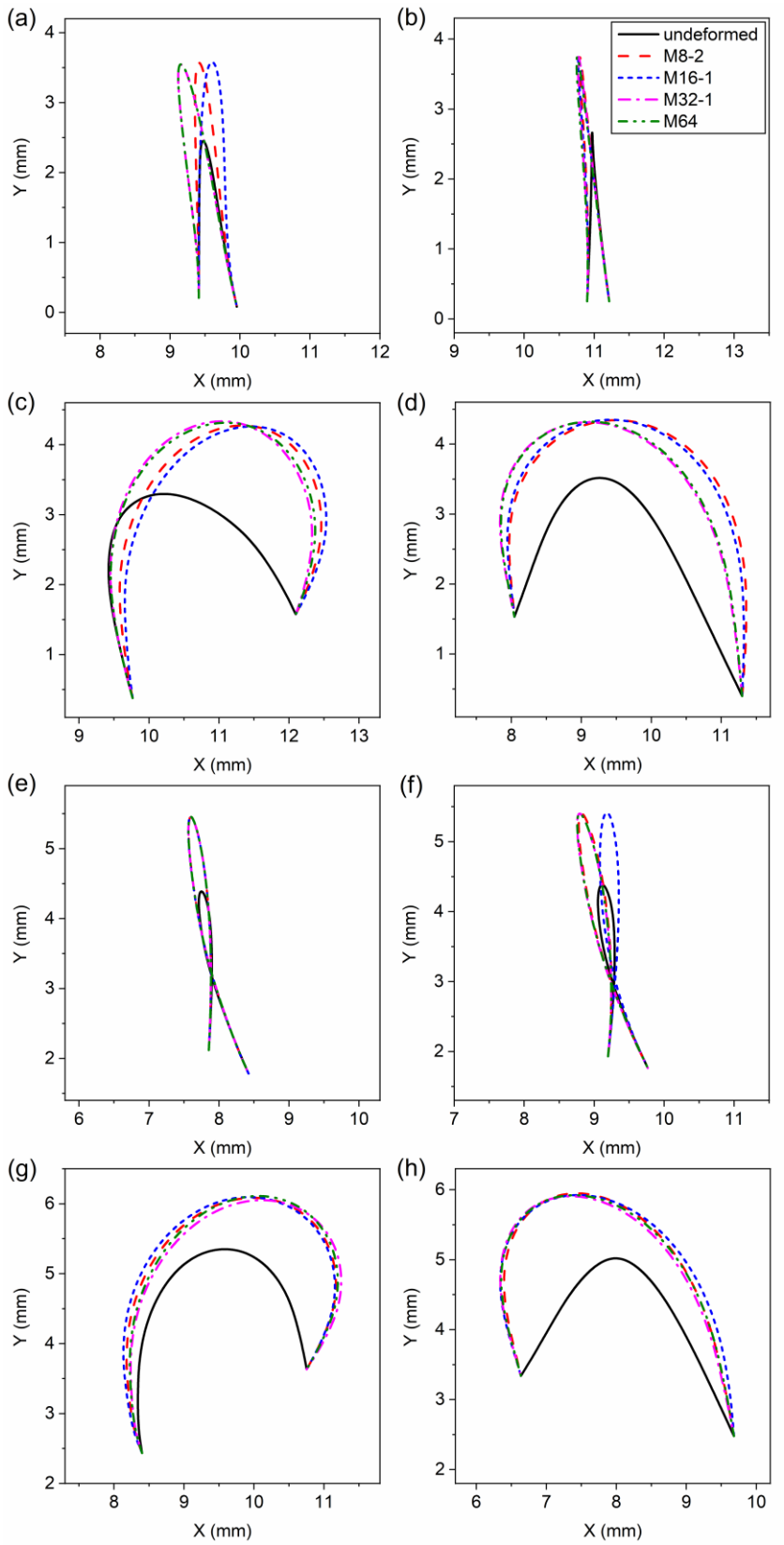

Fig. 15. Projections of deformed spacer monofilaments of U2 in the X-Y plane at displacement of 2.5 mm for FE models with different number of unit cells: (a)v1; (b)v2; (c)i3; (d)i4; (e)v5; (f)v6; (g)i7; (h)i8.

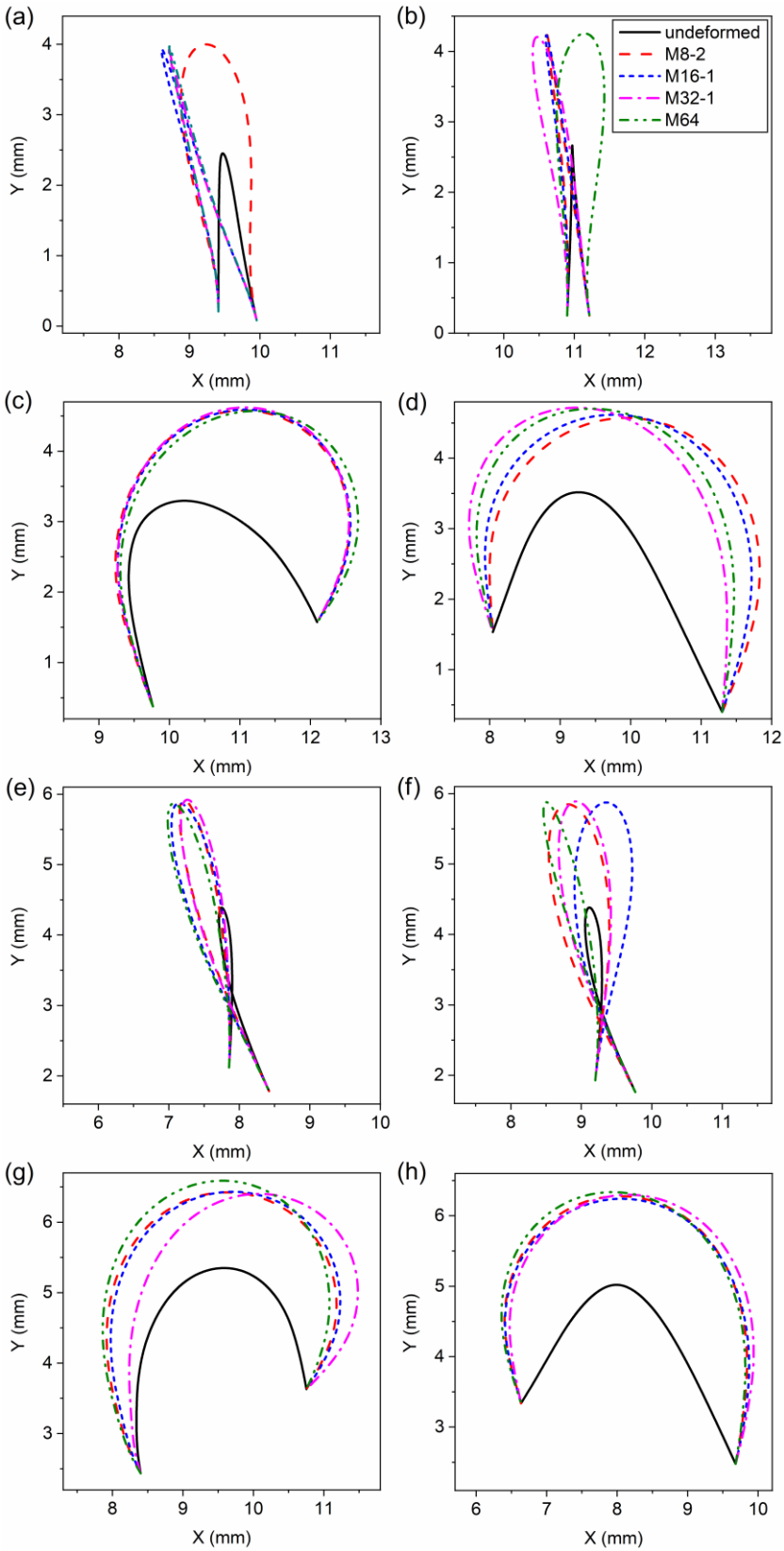

Fig. 16. Projections of deformed spacer monofilaments of U2 in the X-Y plane at displacement of 5 mm for FE models with different number of unit cells: (a)v1; (b)v2; (c)i3; (d)i4; (e)v5; (f)v6; (g)i7; (h)i8.

Significant differences in projections of the spacer yarns among the four models at the displacement of 5 mm are found in Fig. 16. In addition to rotation, clear torsional deformations can be observed on both vertical and inclined spacer yarns. For example, v1 of M8-2 in Fig. 16(a) has the biggest enclosed area among the four models, implicating the largest torsional deformation. In addition, the enclosed area of v6 decreases as the number of unit cell increases (Fig. 16(f)). The projections of i4 and i7 differ substantially in different FE models as shown in Fig. 16(d) and (g), which is caused by the interactions among spacer yarns.

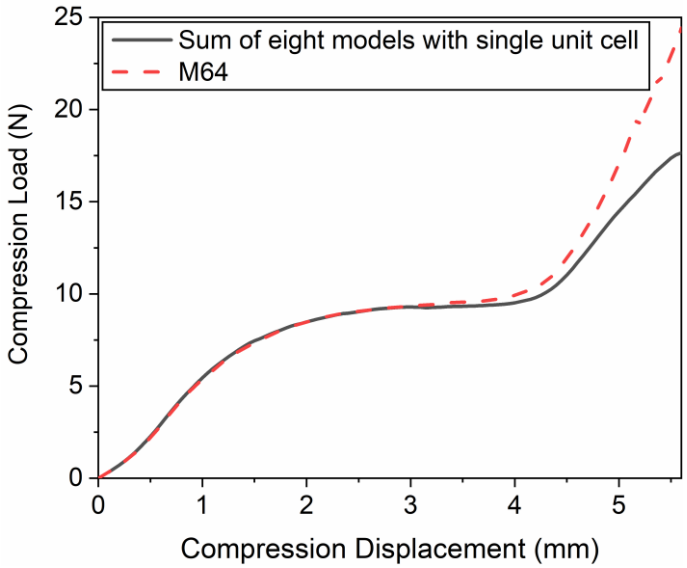

Fig. 17. Compression load–displacement curves of FE models with or without interactions among unit cells.

It can be seen from the VMS plots and projections in the X-Y plane that interactions among spacer yarns in the densification stage are more significant than those in the linear and plateau stages. Fig. 17 compares the compression loads between the sum of the eight FE models built with single unit cell and M64 with eight unit cells. The former is the sum of the eight curves presented in Fig. 11(a) except the experimental

curve. In this way, the two simulated compression load–displacement curves were generated based on the same spacer yarns, but the interactions among unit cells were neglected for the sum of eight FE models. This comparison further proves that interactions among unit cells have critical influence on the compression resistance in the densification stage.

5. Conclusions

A FE analysis on the compression behavior of a typical spacer fabric structure by considering the geometric variations and number of spacer monofilaments was conducted based on the precise geometry reconstructed from μCT scanning. The following conclusions can be drawn.

(1) Both the vertical and inclined spacer yarns are different in their length, enclosed area of planar projections, curvature and torsion. The curvatures of spacer yarns gradually increase from their two ends and reach a fluctuant region in the middle section. The torsions of spacer yarns are highly fluctuant and can be positive and negative with different directions of twisting.

(2) Geometric variations of spacer yarns and different numbers or combinations of unit cell can produce similar compression load–displacement curves with three distinct stages, but the geometric variations can bring about different compression load levels in the three stages. Lower length, enclosed area, curvature and torsion of spacer yarns can result in a higher compression load.

(3) The main deformation mode of spacer yarns in the linear elasticity and plateau stages is rotation, while torsional deformation dominates in the densification stage.

Contacts among spacer yarns are more significant and play an important role in affecting the compression behavior in the final densification stage.

Acknowledgment

The work described in this paper is sponsored by the National Natural Science Foundation of China (11702062), Shanghai Pujiang Program (17PJ1400300), Fundamental Research Funds for the Central Universities (16D110120), and initial research funds for Young Teachers of Donghua University (101-07-0053036).

Data availability

The raw data required to reproduce these findings are available to download from [http://dx.doi.org/10.17632/9jhrcvd893.1].

References

1. Liu YP, Hu H. Compression property and air permeability of weft-knitted spacer fabrics. J Text Inst 2011;102(4):366–372.
2. Ye X, Fangueiro R, Hu H, Araújo M. Application of warp-knitted spacer fabrics in car seats. J Text Inst 2007;98(4):337–343.
3. Rajan TP, Souza LD, Ramakrishnan G, Zakriya GM. Comfort properties of functional warp-knitted polyester spacer fabrics for shoe insole applications. J Ind Text 2016;45(6):1239–1251.
4. Yip J, Ng SP. Study of three-dimensional spacer fabrics: molding properties for intimate apparel application. J Mater Process Technol 2009;209:58–62.
5. Liu YP, Hu H, Zhao L, Long HR. Compression behavior of warp-knitted spacer

fabrics for cushioning applications. Text Res J 2012;82(1):11–20.

6. Liu YP, Hu H, Long HR, Zhao L. Impact compressive behavior of warp-knitted spacer fabrics for protective applications. Text Res J 2012;82(8):773–788.
7. Chang YP, Ma PB, Jiang GM. Energy absorption property of warp-knitted spacer fabrics with negative Possion's ratio under low velocity impact. Compos Struct 2017;182:471–477.
8. Armakan DM, Roye A. A study on the compression behavior of spacer fabrics designed for concrete applications. Fiber Polym 2009;10(1):116–123.
9. Liu YP, Hu H. Vibration isolation behaviour of 3D polymeric knitted spacer fabrics under harmonic vibration testing conditions. Polym Test 2015;47:120–129.
10. Koeckritz U, Cherif CH, Weiland S, Curbach M. *In-situ* polymer coating of open grid warp knitted fabrics for textile reinforced concrete application. J Ind Text 2010;40(2):157–169.
11. Zhi C, Long HR, Sun FX. Low-velocity impact properties and finite element analysis of syntactic foam reinforced by warp-knitted spacer fabric. Text Res J 2017;87(16):1938–1952.
12. Lu ZQ, Jing XY, Sun BZ, Gu BH. Compressive behaviors of warp-knitted spacer fabrics impregnated with shear thickening fluid. Compos Sci Technol 2013;88:184–189.
13. Supeł B, Mikołajczyk Z. Model of the connector for 3D distance knitted fabric fastened by articulated joints. Fibres Text East Eur 2008;16(5): 77–82.
14. Supeł B, Mikołajczyk Z. Model of the compressing process of a one- and two-side fastened connector of a 3D distance knitted fabric. Fibres Text East Eur 2008;16(6):44–48.

15. Supeł B, Mikołajczyk Z. Modelling the process of the compression of distance knitted fabrics in the aspect of ‘elastica curves’. Fibres Text East Eur 2010;18(4):52–55.
16. Mokhtari F, Shamshirsaz M, Latifi M, Maroufi M. Compressibility behaviour of warp knitted spacer fabrics based on elastic curved bar theory. J Eng Fiber Fabr 2011;6(4):23–33.
17. Chen MY, Lai K, Sun RJ, Zhao WZ, Chen X. Compressive deformation and load of a spacer filament in a warp-knitted spacer fabric. Text Res J 2017;87(5):631–640.
18. Vassiliadis S, Kallivretaki A, Psilla N, Provatidis Ch, Mecit D, Roye A. Numerical modelling of the compressional behaviour of warp-knitted spacer fabrics. Fibres Text East Eur 2009;17(5):56–61.
19. Brisa VJD, Helbig F, Kroll L. Numerical characterisation of the mechanical behaviour of a vertical spacer yarn in thick warp knitted spacer fabrics. J Ind Text 2015;45(1):101–117.
20. Hou XN, Hu H, Liu YP, Silberschmidt V. Nonlinear compression behavior of warp-knitted spacer fabric: effect of sandwich structure. CMC-Comput Mat Contin 2011;23(2):119–134.
21. Hou XN, Hu H, Silberschmidt V. A study of computational mechanics of 3D spacer fabric: factors affecting its compression deformation. J Mater Sci 2012;47:3989–3999.
22. Sun FX, Ma MY, Pan XX, Liu G, Yang S, Zheng DM, Li M, Du ZQ. Simulation of plate compression behavior of warp-knitted spacer fabrics based on geometry and property parameters. Text Res J 2019;89(6):1051–1064.
23. Orlik J, Pietsch K, Fassbender A, Sivak O, Steiner K. Simulation and

experimental validation of spacer fabrics based on their structure and yarn's properties. Appl Compos Mater 2018;25:709–724.

24. Liu YP, Hu H. Finite element analysis of compression behavior of 3D spacer fabric structure. Int J Mech Sci 2015;94-95:244–259.
25. Liu YP, Hu H. An experimental study of compression behavior of warp-knitted spacer fabric. J Eng Fiber Fabr 2014;9:61–69.
26. Aronov B, Peled SH, Knauer C, Wang Y, Wenk C. Fréchet distance for curves, revisited. Lect Notes Comput Sci 2006;4168:52–63.
27. Zhang S, Li J. Anisotropic elastic moduli and Poisson's ratios of a poly (ethylene terephthalate) film. J Polym Sci Part B: Polym Phys 2004;42:260–266.
28. Mott P, Roland C. Limits to Poisson's ratio in isotropic materials. Phys Rev B 2009;80:132104.